International Journal of Mass Spectrometry 289 (2010) 92–97

Contents lists available at ScienceDirect

International Journal of Mass Spectrometry

journal homepage: www.elsevier.com/locate/ijms

Ultrafast dynamics of pyridine in "channel three" region

Bingxing Wang[a,b], Benkang Liu[a,b], Yanqiu Wang[a], Li Wang[a,*]

[a] State Key Laboratory of Molecular Reaction Dynamics, Dalian Institute of Chemical Physics, Dalian 116023, China
[b] Graduate School of the Chinese Academy of Sciences, Beijing 100049, China

ARTICLE INFO

Article history:
Received 12 May 2009
Received in revised form
18 September 2009
Accepted 28 September 2009
Available online 7 October 2009

Keywords:
Time resolved photoelectron imaging
Rydberg
Vibrational redistribution

ABSTRACT

The ultrafast dynamics of the S_1 ($n\pi^*$) state of pyridine has been investigated by using femtosecond time-resolved mass spectrometry and photoelectron imaging combined with (1+2′) resonance-enhanced multiphoton ionization via the Rydberg states. Upon excitation into the channel-three region, an ultrafast decay process is observed with a lifetime of about 3.7 ps. The fragment ions show an additional ultrafast decay component. Time resolved photoelectron imaging experiments reveal the excited pyridine in channel three region relaxes to an optically dark state on this short time scale. According to previous experimental and theoretical results, we suggest tentatively the ultrafast channel is due to IVR induced fast internal conversion.

1. Introduction

Photodynamics of azabenzenes had abstracted extensive attention for many years due to its important roles in the UV photodamage of nucleic acids [1]. A special phenomenon in aromatic molecules is the dramatic decrease in the fluorescence quantum yield above the first UV absorption band. For example, at low excess energies (<3000 cm^{-1}) in S_1 of benzene, the fluorescence quantum yield was about 0.2 and the lifetime of vibrational levels ranges from 60 to 120 ns [2]. A sudden increase of the decay rate occurs, while the excess energy is higher than 3000 cm^{-1} [3]. Neither internal conversion (IC), nor intersystem crossing (ISC) to optical dark triplet state were thought to be responsible for the deactivation process, which was referred as "channel three" [4].

The ultrafast decay process of the channel-three behaviour has also been observed in azabenzenes [5–6]. Pyridine, the simplest and the most fundamental azabenzene, has been extensively studied about the photophysics and photochemistry of its low-lying excited states [5–16]. The onset for pyridine is 1600 cm^{-1} above the S_1 origin [6–8].

Since its first observation, channel three had attracted great interest and stimulated many experiments. The first direct observation of the $S_1(n\pi^*)$ decay was performed in 1982 [9]. The nonradiative decay was characterized by fast $S_1 \rightarrow S_0$ IC. The excitation-energy dependence of quantum yields for fluorescence and ISC had been examined [5]. This ultrafast decay may consist of $S_1 \rightarrow S_0$ IC enhanced by participation of the intermediate state, which results in photoisomerization corresponding to the $S_2 \leftarrow S_0$ absorption transition. Sobolewski and Domcke [10] calculated the potential energy surfaces (PES) of the S_0, S_1 ($n\pi^*$) and S_2 ($\pi\pi^*$) states of pyridine along the reaction path leading to the prefulvenic forms. The prefulvenic form was found to adiabatically correlate to the S_2 ($\pi\pi^*$) excitation. The PES of the S_2 ($\pi\pi^*$) state crosses those of the S_1 ($n\pi^*$) and the S_0 states along the reaction path, which is responsible for the channel-three behaviour of pyridine. On the excitation at 271.5 nm, a nonbonding electron on the nitrogen atom is projected on to the antibonding π^* orbital of the ring, and hence weakens the C—N bond resulting in its scission. This channel had been supposed to be responsible for the fast decrease in emission quantum yield. The abrupt onset of the channel-three phenomenon in pyridine corresponded to the energy threshold for the ring-cleavage [11]. A more detailed study was performed in jet-cooled S_1 pyridine [6]. Many theoretical works have been performed to explain this phenomenon of pyridine [10,12–14].

By using femtosecond time-resolved mass spectrometry, the ultrafast dynamics of pyridine in isolated phase was investigated [15]. Upon 277 nm excitation below the channel-three threshold, the transients exhibit two fast decay components of 400 fs and 3.5 ps with a slower one of 15 ps. Later, the excited-state decay pathways after 266 nm excitation were comprehensively studied in liquid phases, by using femtosecond transient absorption spectroscopy [14]. Two decay processes were observed with the time constants of 2.2 and 9–23 ps, respectively. The theoretical calculations show a conical intersection (CI) between the PES of the ground and $S_2(\pi\pi^*)$ state [14]. This CI was found to be responsible for the ultrafast decay of S_2 ($\pi\pi^*$) state with the lifetime of 2.2 ps, leading to the formation of the prefulvenic form. The 9–23

* Corresponding author. Tel.: +86 411 84379243; fax: +86 411 84675584.
E-mail address: liwangye@dicp.ac.cn (L. Wang).

1387-3806/$ – see front matter © 2009 Elsevier B.V. All rights reserved.
doi:10.1016/j.ijms.2009.09.014

ps process corresponds to the nonradiative decay of the excited state S_1 ($n\pi^*$). Recently, the transient structures formed through nonradiative decay of pyridine, were directly determined by using the ultrafast electron diffraction [11,16]. Upon 266 nm excitation a ring-opened diradical structure was observed and formed in 17 ps. Ring-opening process had been suggested to be dominant in the channel-three dynamics of pyridine [11,16].

Femtosecond time-resolved photoelectron spectroscopy had been proven powerful methods for studying the ultrafast excited-state dynamics [17–19]. The lifetime at the S_1 ($n\pi^*$) origin of pyridine was measured via the singlet 3s and 3p Rydberg states by ($1+1'+1'$) real time scale pump–probe methods [20].

To the best of our knowledge, few works [11,16] are focused on the femtosecond time-resolved channel-three behaviour of pyridine. In this letter, we investigate directly the ultrafast decay process of pyridine just above the threshold for the channel three [6]. The ($1+1'+1'$) multiphoton ionization scheme is employed for ionization and enhanced by the resonance with 3s and 3p Rydberg states. Time-resolved photoelectron imaging (TRPEI) is applied for obtaining the photoelectron kinetic energy distributions along with the decay process of the excited pyridine. The time evolution of the initially prepared excited state is monitored by femtosecond-resolve mass spectrometry.

2. Experimental method

The experimental setup for the femtosecond time-resolved mass spectrometry and the velocity map imaging setup has been described elsewhere in detail [21]. We just give a brief description here.

Our homebuilt solid-state femtosecond laser system consists of a seed oscillator, an amplifier with a stretcher and a compressor. The fundamental light is centered at 814 nm (with ~30 nm bandwidth, 70 fs pulse width, 20 Hz repetition rate). The third harmonic generation of the fundamental light, centered at 271.5 nm, is served as the pump pulse. The probe pulse is the second harmonic generation at 407.1 nm. The pump beam is temporally delayed with respect to the probe beam by a computer-controlled step-motor driven linear translator (Sigma Koki, SGSP26-150). The two laser beams are collinearly combined by a dichroic mirror and introduced into the vacuum chamber with a fused silica lens f = 380 and 450 mm, respectively. The cross-correlation function between the pump and probe pulses measured with Xe is estimated to be ca. 83 fs. The polarizations of the two beams were aligned parallel to the detector plane, and perpendicular to the molecular beam. The polarization of the pump laser can be varied with a Berek polarization compensator (Model 5540).

The time of flight mass spectrometer is a typical Wiley-McLaren machine. Commercial pyridine (99.5%, without further purification) is mixed with the carrier gas helium (1.3 atm to vacuum, with a tiny amount of Xe in the carrier gas). The seeded gas sample is expanded through a pulsed valve (General Valve, with 0.5 mm orifice), into the ionization accelerating region, 5 cm downstream from the nozzle. Ions in this region are extracted and accelerated by a typical three electrodes system, and detected by a two-stage microchannel plate (MCP) detector at the end of the flight tube. Output of MCP is fed into a digital oscilloscope (Tektronix Inc., TDS3054B), GPIB interfaced with a computer. Each TOF mass spectrum is the average result over 532 laser shots. The pump–probe transient corresponds to an average of more than 12 scans. With molecular beam on, the source chamber and flight chamber are maintained at 1.5×10^{-4} and 6×10^{-6} Pa, respectively.

In the TRPEI experiment, photoelectrons are extracted into the field-free region, which is doubly shielded against stray magnetic fields with a μ-metal tube. At the end of TOF tube, the electrons strike a two-stage MCP detector backed by a phosphor screen. The images on the screen are captured with a thermoelectrically cooled charge-coupled-device (CCD) video camera (Lavision Inc., Imager QE). Each image corresponds to the accumulation of 10,000 laser shots. The emission from the phosphor screen is monitored by a photomultiplier connected to the digital oscilloscope. An inverse-Abel transform is applied to calculate slices through the three-dimensional (3D) photoelectron distributions from the measured two-dimensional (2D) raw images.

3. Results and discussion

To avoid one-color multiphoton ionization, the foci of both lasers are placed after crossing the molecular beam. The fragment ions can originate from the fragmentation of the molecular ion, or from the ionization of an excited neutral fragment during the time interval between the pump and the probe.

3.1. Time-resolved photoelectron imaging

TRPEI can allow for direct identification of the electronic states involved in the ultrafast processes. As reported in Ref. 20, ultrafast electronic dephasing from the S_1 ($n\pi^*$) state of the n = 3 Rydberg states of pyridine was studied by time-resolved photoelectron imaging in conjunction with ($1+2'$) resonance-enhanced

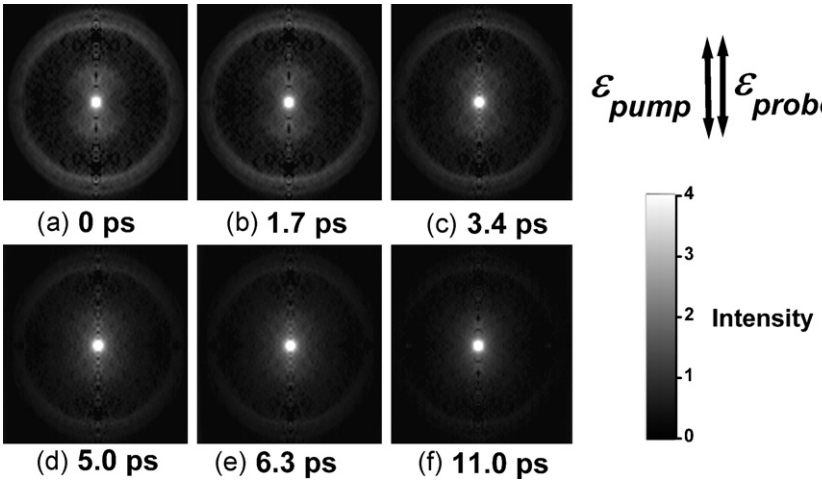

Fig. 1. Time-resolved photoelectron images (inverse-Abel transform) of pyridine at given pump–probe delay time. Pump and probe light intensities are 6.8×10^{10} and 8.9×10^{11} W/cm^2, respectively. Polarization of the two laser beams is parallel to each other and in the plane of the figure.

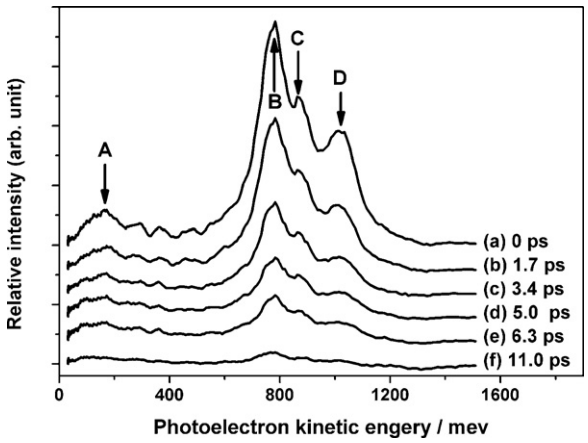

Fig. 2. Photoelectron kinetic energy distributions extracted from Fig. 1 at given delay time. The peak A–D corresponds to 172, 783, 872 and 1015 meV, respectively, fitted by Lorentzian profiles.

multiphoton ionization (REMPI) via the S_1 state. Two-photon ionization from the S_1 state was enhanced by the resonance with singlet 3s (n^{-1}) and 3p (n^{-1}) Rydberg states of pyridine. The same pump–probe schedule is applied for investigating the electronic dephasing of pyridine populated in its channel three region. Fig. 1 shows photoelectron images at different pump–probe delay times. To avoid the unwanted one-color multiphoton transition and ionization, both the pump and probe light intensities are kept to be weaker and estimated to be 6.8×10^{10} and 8.9×10^{11} W/cm^2, respectively.

Kinetic energy distributions of the photoelectrons, extracted from the raw images presented in Fig. 1 at given delay time, are illustrated in Fig. 2. Three sharp peaks (B, C and D, indicated in the figure) center at 783, 872 and 1015 meV, respectively. Peak (A), centered at 172 meV, is broad and blurry, compared with other three peaks. Following the assignment method in Ref. [20], these four peaks are attributed to ionization from 3s and 3p (x, y, z components) Rydberg states, populated via $1 + 1'$ excitation schedule.

Different from the case of pyrazine [22], no other peak arises along the pump–probe delay time, while these four components diminish rapidly. This means pyridine excited by 271.5 nm relaxes to an optically dark state via intersystem crossing or to hot S_0 via internal conversion, which cannot be ionized in current experimental setup. The component with energy less than 172 meV is tiny and blurry, might be due to the ionization from triplet state, as suggested in Ref. [20]. Pyridine after undergoing IC to the S_0 state can hardly be ionized, since no resonant state can be populated via one-photon electronic transition from S_0.

The energetic of the zero vibrational levels, T(Rydberg) in resonance can be deduced easily from the energy conservation [20]:

$$\mathrm{PKE} = T(\mathrm{Rydberg}) + h\nu_2 - \mathrm{IE} = h\nu_2 - \frac{R}{(n-\delta)^2} \quad (1)$$

where ν_2 are the probe laser frequencies; IE is the adiabatic ionization energy; R is the Rydberg constant; n is the principal quantum number of the Rydberg state; and δ is the quantum defect. The

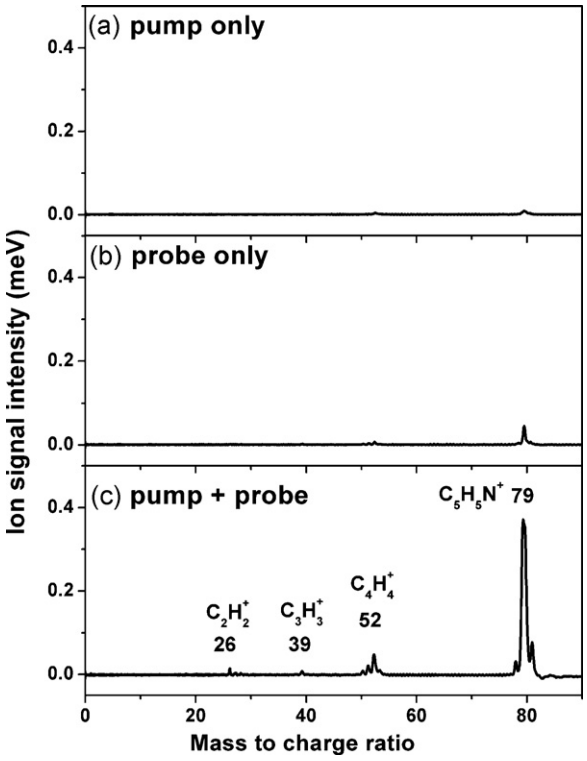

Fig. 3. Mass spectra recorded (a) with only pump laser, (b) with only probe laser, and (c) with pump and probe laser at zero delay time. Pump laser and probe laser are 1.6×10^{11} and 9.3×10^{11} W/cm^2, respectively.

energies of Rydberg states and corresponding quantum defects, calculated with the accurate IE measured recently [23], are listed in Table 1. From comparison with the calculated energies by MRD-CI method [24] and the recently experimental results by TRPEI [20], the Rydberg states observed here are assigned as in Table 1. For the 3s Rydberg state, the energy value we obtained is almost the same as that in the TRPEI result [20]. The energy of $3p_z$ Rydberg state is in agreement with VUV result [24] and is higher than the previous TRPEI value [20].

The time evolution of the total photoelectron signal can be fitted with the same time constant of about 3.7 ps as that in the mass spectrometry.

3.2. Femtosecond mass spectrum and pump–probe transients

Fig. 3 displays the TOF mass spectra, pumped by 271.5 nm and probed by 407.1 nm. The power intensities of the pump and probe beams at the interaction region are estimated to be 1.6×10^{11} and 9.3×10^{11} W/cm^2, respectively. The mass spectra of pyridine with pump light and probe light only are illustrated in Fig. 3(a and b), respectively. Excitation of pyridine at 271.5 nm cannot lead to dissociation [25], as illustrated in Fig. 3(a) with the pump light only. Tiny fragment signal of 52 amu can be found in Fig. 3(b) with the probe light only. This fragment ion should be from dissociative ionization of neutral pyridine. Recent VUV experiment [26] indicated

Table 1
Assignment of the Rydberg states of pyridine. The photoelectron kinetic energies (PKE) are derived from Fig. 2. The quantum defects (δ) and the energies (T) of Rydberg states are calculated with Formula (1).

	State	PKE (meV)	T (cm^{-1}) (δ)	T (cm^{-1}) (δ) [20]	MRD-CI [24]	VUV [24]
A	3s	172	51,008 (0.82)	51,020 (0.85)	49,911	50,650
B	$3p_z$	783	55,936 (0.55)	55,390 (0.62)	54,049	55,890
C	$3p_x$	872	56,654 (0.50)	56,120 (0.57)	55,081	
D	$3p_y$	1,015	57,807 (0.41)	57,140 (0.50)	57,041	

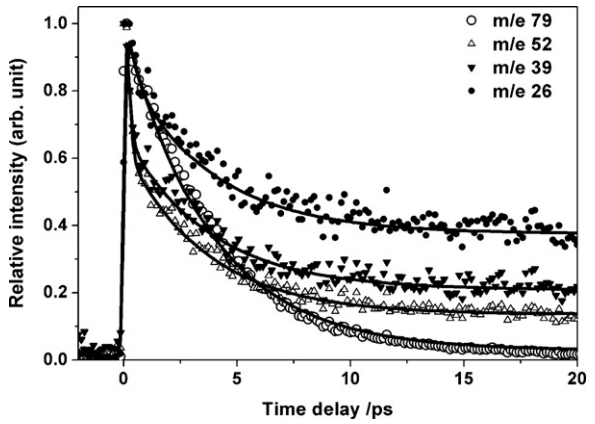

Fig. 4. The pump–probe delay profiles of pyridine and different fragment ions. The pump and probe intensities are the same as those in Fig. 3. Open circles show the observed raw data points. The solid lines are the fit curves of biexponential decay components.

that single photo ionization of pyridine resulted in the fragmentation to 52 amu. Fig. 3(c) shows the time-of-flight mass spectrum, taken at zero time delay between the pump and probe. The spectrum shows the parent ion is dominant and there are relatively weak fragment ions peaks. No van der Waals cluster ions, such as $(C_5H_5N)_n$, can be observed under our experimental condition. In the pump–probe schedule, both fragment ions and parent ions were enhanced, as shown in Fig. 3(c). Peaks at 52, 39 and 26 amu correspond to $C_4H_4^+$, $C_3H_3^+$ and $C_2H_2^+$, respectively [26–27].

Transient signals of these ions are illustrated in Fig. 4. The transient signals can be well fitted by two exponential decay components with a constant component, which corresponds to longer lifetime, estimated to be nanosecond scale. Lifetimes of the two decay components are about 330 fs and 3.7 ps, respectively. The fitting parameters are list in Table 2. Note the ratio of fs to ps components is small in the decay profile of pyridine parent (79 amu), and the parent ion transient signal can be well fitted by single picosecond decay component, which gives almost the same lifetime constant. In the case of fragment ions, two components must be applied for fitting the curves. This is different from the dissociative ionization model, in which all fragment ions would follow the same model as the parent ion.

We notice the intensity of the pump light may modify the ratio of fs to ps components, both in the parent ion and fragment ion signals. The decay profiles of pyridine and the main fragment ions (52 amu) with different pump laser intensities are illustrated in Fig. 5(a and b). Fitting results of the profiles by two exponential decay component model, time constants and amplitudes, are listed in Table 3. It is evident the ratio of fs to ps component is sensitive to the pump laser intensity. Contribution of the fast decay component increases with the pump laser intensity. This observation, however, seems to conflict with the common sense that excited dynamics is independent of the excitation intensity.

Table 2
Time constants and amplitudes given by fit of the experimental data for pyridine molecule and fragments with pump and probe laser intensities, 1.6×10^{11} and 9.3×10^{11} W/cm^2, respectively. Fitting model: $A_1 \times \exp(-t/\tau_1) + A_2 \times \exp(-t/\tau_2) + A_3$.

m/e	Species	τ_1 (ps)	τ_2 (ps)	$A_1/(A_1+A_2+A_3)$	$A_3/(A_1+A_2+A_3)$
79	$C_5H_5N^+$	0.28 ± 0.13	3.54 ± 0.12	0.15	0.01
52	$C_4H_4^+$	0.11 ± 0.01	3.53 ± 0.14	0.53	0.10
39	$C_3H_3^+$	0.12 ± 0.02	3.67 ± 0.21	0.43	0.18
26	$C_2H_2^+$	0.39 ± 0.20	3.74 ± 0.31	0.16	0.37

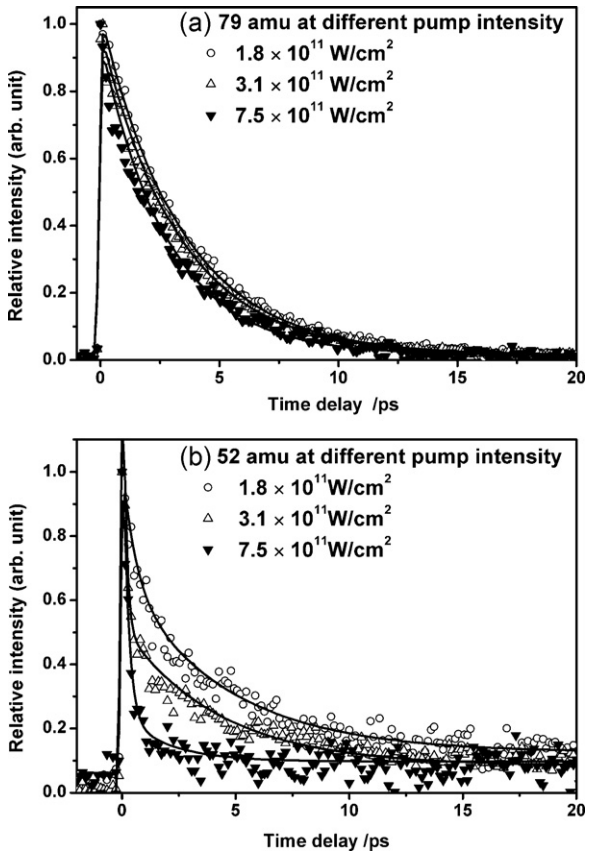

Fig. 5. The pump–probe delay profiles of pyridine and fragments (52 amu) at different pump laser intensities. The probe laser intensity is kept at 9.3×10^{11} W/cm^2. Open circles show the observed raw data points. The solid lines are the fit curves of biexponential decay components.

3.3. Discussions

Three possible deactivation processes may occur from the S_1 state of pyridine: S_1 to S_0 fluorescence decay (FI), internal conversion to S_0 (IC), and intersystem crossing to optical dark triplet state (ISC). Low fluorescence yield (5.9×10^{-5}) was observed and the ISC quantum yield was measured to be 0.3 upon excitation into $S_1(n\pi^*)$ (0–0 at 287.6 nm) [9], and ISC yield dramatically decreased to 0.02 [6] when excited at 271.5 nm. Therefore, the dominant de-excitation process of pyridine in its "channel three" region is the internal conversion to S_0, and the contribution of ISC to the total de-excitation of S_1 should be minor. The minor constant signal at long delay time in Fig. 3 may be due to the ionization from the triplet state populated via ISC. This process also appears as a low-energy component (less than 170 meV) in Fig. 2, similar to reported observations [20], excited at 287.5 nm and 283 nm.

Pyridine excited at 277 nm (with 1300 cm^{-1} excess energy above the S_1 origin, below the channel-three threshold) had been investigated by femtosecond time-of-flight mass spectrometry [15]. At 277 nm excitation, the pyridine parent ion and fragment ion (52 amu) transient exhibit two fast decay components of 400 fs and 3.5 ps with a slower one of 15 ps [15]. The 400 fs component was assigned to the initial displacement of the wavepacket and intramolecular vibrational energy distribution (IVR) [15], and isomerization to Dewar and Hückel structures occurs on this time scale. The 3.5 and 15 ps ones were attributed to the rearomatization of the Dewar and Hückel isomers to the hot pyridine, respectively [15]. The ultrafast electron diffraction has been used to determine the transient structures formed through nonradiative decay of S_1 ($n\pi^*$) of pyridine at 266 nm excitation [11,16]. The result showed a

Table 3
Time constants and amplitudes extracted from the experimental data for pyridine excited by different pump laser intensities. The probe laser intensity is 9.3×10^{11} W/cm^2. Fitting model: $A_1 \times \exp(-t/\tau_1) + A_2 \times \exp(-t/\tau_2) + A_3$.

Pump intensity ($\times 10^{11}$ W/cm^2)	τ_1 (ps) (m/e 79)	τ_2(ps) (m/e 79)	A_1/A_2 (m/e 79)	τ_1 (ps) (m/e 52)	τ_2 (ps) (m/e 52)	A_1/A_2 (m/e 52)
1.8	0.28 ± 0.10	3.49 ± 0.07	0.14	0.13 ± 0.07	3.86 ± 0.22	0.35
3.1	0.28 ± 0.06	3.54 ± 0.10	0.33	0.13 ± 0.02	4.00 ± 0.36	1.76
7.5	0.28 ± 0.04	3.53 ± 0.10	0.50	0.13 ± 0.03	3.33 ± 1.01	4.50

ring-opened diradical structure that was formed in 17 ps. 266 nm and 277 nm excited pyridine into different regions, both in the S_1 electronic state, above and below the channel three threshold, respectively. It seems to be reasonable that upon 266 nm excitation, a new reactive channel is accessible to open, which is different from the case of 277 nm excitation [15]. No fragments had been observed, excited by 266 nm [11,16], while fragment ions (52 amu) were the dominant dissociation product in the case of 277 nm excitation [15].

Following femtosecond 271.5 nm excitation (with bandwidth 380 cm^{-1} FWHM), pyridine can be superexcited into $6a_0^3$ (274.6 nm), $Y_0^1 6a_0^1 12_0^1$ (273 nm), $Y_0^1 6a_0^3$ (272.6 nm), 12_0^2 (271.9 nm) and $6a_0^2 12_0^1$ (271.3 nm) vibrational bands [6], with about 2000 cm^{-1} excess energy above the S_1 origin. The absorption spectrum around 271 nm [6] is much broader than those around 287.5 nm [20], 283 nm [20] and 277 nm [15], which means the lifetime of vibrational levels in this region is much shorter than those at the reported excitation region [11,15,20]. As suggested in Ref. [6], photophysical properties of the S_1 state of pyridine is governed by IVR induced internal conversion to S_0. The threshold of channel three is consistent with the onset of the very rapid IVR. Similar "channel-three-like" behaviour of isoquinoline had been investigated [28]. At an energy about 1600 cm^{-1} above the origin of the S_1 state of isoquinoline, the level density was about 7 cm^{-1}, which was believed to be sufficient for IVR to take place [28]. We apply the same calculation method, the Beyer-Swinehart algorithm [29], to estimate the density of vibrational states of pyridine in its S_1 state. The complete-active-space self-consistent-filed (CASSCF) method is used for the S_1 excited state, which is implemented in the Gaussian 03 program package [30]. The active space includes four occupied π orbitals, one occupied n orbital (the lone pair of nitrogen atom), and three unoccupied π^* orbital, designated as (10, 8). The geometry optimization and the vibrational frequency analysis of the S_1 state are performed

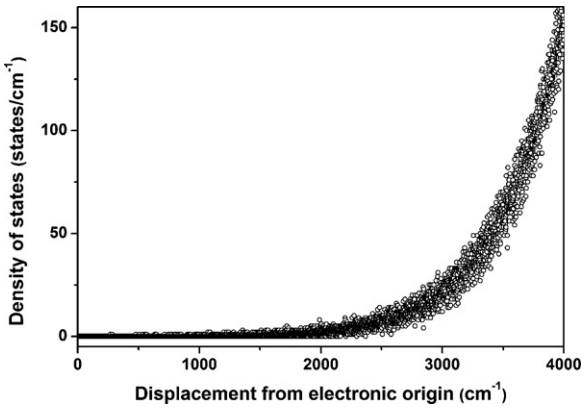

Fig. 6. The density of the vibronic states in the S_1 state up to 4000 cm^{-1}.

at CASSCF (10, 8)/6-311+G (d, p) level. Harmonic vibrational frequencies are also calculated in order to characterize the stationary point (no imaginary frequency), which is used in the computation of the density of vibrational state. Twenty-seven S_1 vibrational fundamentals are used in the computation of the density of vibrational state. The calculation result, illustrated in Fig. 6, shows that, at about 2000 cm^{-1} above the S_1 origin, corresponding to our experiment, the level density (about 5 cm^{-1}) is large enough for IVR to occur. The actual density of the vibrational state of the S_1 state might be greater than this value, since the strong S_2–S_1 vibronic coupling may lower the vibrational frequencies of the out-of-plane modes, resulting in an increase in the level density, simlar to the case of isoquinoline [28]. The IVR process populates crucial out-of-plane bending mode, which leads to a rapid $S_1 \rightarrow S_0$ internal conversion. In our experiment, the lifetime of the S_1 excited state populated by 271.5 nm excitation is about 3.6 ps.

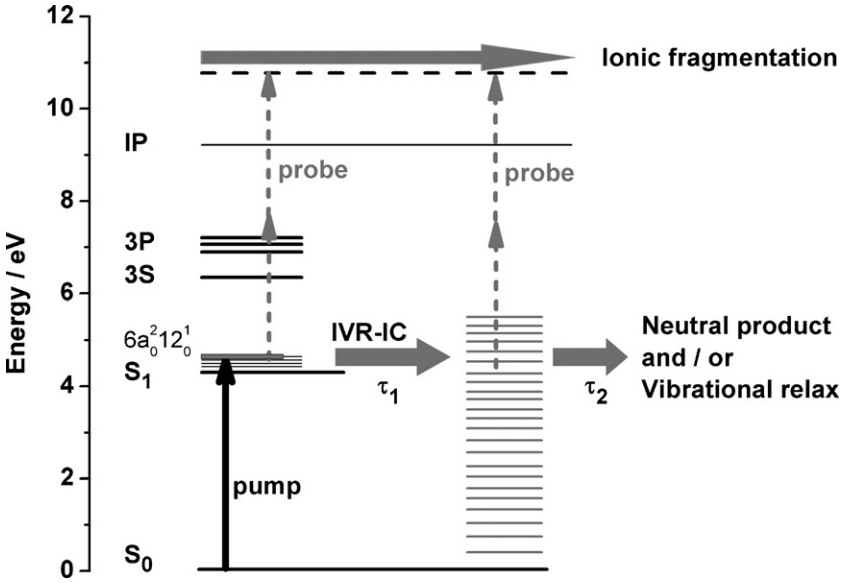

Fig. 7. Possible dynamical processes of pyridine occured in channel three region.

Although several de-excitation channels from pyridine $S_1(n\pi^*)$ had been proposed, for example, isomerization to Dewar's, Hückel's, prefulvenic structures, etc. [15], it is difficult to tell the differences among these structures by ionization detection methods. The fragment ions observed in our experiments implies that ring-opening channel to form diradical product perhaps is the main dissociation channel, besides the dominant internal conversion to S_0. Isomerization to the Dewar and Hückel structures of pyridine was supposed to be minor channel [11], following the excitation at 266 nm.

We notice the difference in transient profiles between parent ions and fragment ions in Fig. 4. The parent ion transient signal can be well fitted by single picosecond decay component, while fragment ions must be fitted by two decay components. As mentioned above, the main de-excitation of pyridine S_1 is due to IVR induced internal conversion, the difference in transient signals of parent and fragment ions may be due to the difference of the ionization cross-section. If the cross-section for ionization of the parent from the optical bright states and the dark states after intramolecular vibrational energy redistribution (IVR) were the same, the pump–probe experiment would not be able to monitor the direct IVR time evolution after coherent excitation from the bright to the dark states. This maybe is the reason why the ratio of fs to ps components is very small in the decay profile of pyridine parent (79 amu).

In our transients, the plateau represents a pyridine species with nanosecond lifetime. This long-lived state must have a smaller ionization cross-section than the originally excited wavepacket. This long-lived state might be due to the ionization of the triplet state, as assigned in previous reports [20,31]. Differences in intensities and profiles are due to different dissociation cross-sections favoring particular dissociation channels [32]. We illustrated the ultrafast process occurred in the pyridine S_1 state in its channel three region in Fig. 7.

4. Conclusions

The ultrafast dynamics of the S_1 ($n\pi^*$) state of pyridine has been investigated by applying femtosecond time-resolved mass spectrometry and photoelectron imaging method combined with (1 + 2′) REMPI via the Rydberg states. Upon excitation into the channel-three region, an ultrafast decay of the S_1 ($n\pi^*$) state is observed with the lifetime of about 3.7 ps. TRPEI experiments reveal the excited pyridine relaxes to an optically dark state on this short time scale. According to previous experimental and theoretical results, we suggest tentatively the ultrafast channel is due to IVR induced fast internal conversion. Additionally, we have assigned the electronic energies of the Rydberg states with the more accurate IE [23]. However, the technique used in this study is unable to give the structure information. Besides, some dynamics information will be lost if the probe pulse cannot ionize the evolutive system across the entire reaction coordinate. Higher energy probe pulses are thus anticipated to provide more details about this ultrafast dynamics.

Acknowledgement

The authors would like to thank the financial support from the National Natural Science Foundation of China (Grant Nos. 20633070 and 20473090).

References

[1] C.E. Crespo-Hernandez, B. Cohen, P.M. Hare, B. Kohler, Chem. Rev. 104 (2004) 1977–2019.
[2] C.S. Parmenter, M.W. Schuyler, Chem. Phys. Lett. 6 (1970) 339–341.
[3] J.H. Callomon, J.E. Parkin, R. Lopez-Delgado, Chem. Phys. Lett. 13 (1972) 125–131.
[4] U. Schubert, E. Riedle, H.J. Neusser, E.W. Schlag, J. Chem. Phys. 84 (1986) 6182–6189.
[5] I. Yamazaki, T. Murao, T. Yamanaka, K. Yoshihara, Faraday Discuss. Chem. Soc. (1983) 395–405.
[6] E. Villa, A. Amirav, E.C. Lim, J. Phys. Chem. 92 (1988) 5393–5397.
[7] E.C. Lim, Adv. Photochem. 23 (1997) 165–211.
[8] P. Avouris, W.M. Gelbart, M.A. El-Sayed, Chem. Rev. 77 (1977) 793–833.
[9] I. Yamazaki, T. Murao, K. Yoshihara, M. FujiTa, K. Sushida, H. Baba, Chem. Phys. Lett. 92 (1982) 421–424.
[10] A.L. Sobolewski, W. Domcke, Chem. Phys. Lett. 180 (1991) 381–386.
[11] R. Srinivasan, J.S. Feenstra, S.T. Park, S.J. Xu, A.H. Zewail, Science 307 (2005) 558–563.
[12] A.L. Sobolewski, E.C. Lim, W. Siebrand, Int. J. Quantum Chem. 39 (1991) 309–324.
[13] M.D. Su, J. Phys. Chem. A 111 (2007) 971–975.
[14] M. Chachisvilis, A.H. Zewail, J. Phys. Chem. A 103 (1999) 7408–7418.
[15] D.P. Zhong, E.W.G. Diau, T.M. Bernhardt, S. De Feyter, J.D. Roberts, A.H. Zewail, Chem. Phys. Lett. 298 (1998) 129–140.
[16] V.A. Lobastov, R. Srinivasan, B.M. Goodson, C.Y. Ruan, J.S. Feenstra, A.H. Zewail, J. Phys. Chem. A 105 (2001) 11159–11164.
[17] O. Gessner, A.M.D. Lee, J.P. Shaffer, H. Reisler, S.V. Levchenko, A.I. Krylov, J.G. Underwood, H. Shi, A.L.L. East, D.M. Wardlaw, E.t.H. Chrysostom, C.C. Hayden, A. Stolow, Science 311 (2006) 219–222.
[18] A. Stolow, A.E. Bragg, D.M. Neumark, Chem. Rev. 104 (2004) 1719–1757.
[19] V. Blanchet, M.Z. Zgierski, T. Seideman, A. Stolow, Nature 401 (1999) 52–54.
[20] M. Tsubouchi, T. Suzuki, J. Phys. Chem. A 107 (2003) 10897–10903.
[21] W. Guo, J. Zhu, B. Wang, Y. Wang, L. Wang, Phys. Rev. A 77 (2008) 033415.
[22] L. Wang, H. Kohguchi, T. Suzuki, Faraday Discuss. 113 (1999) 37–46.
[23] M. Riese, Z. Altug, J. Grotemeyer, Phys. Chem. Chem. Phys. 8 (2006) 4441–4448.
[24] I.C. Walker, M.H. Palmer, A. Hopkirk, Chem. Phys. 141 (1989) 365–378.
[25] M.F. Lin, Y.A. Dyakov, C.M. Tseng, A.M. Mebel, S.H. Lin, Y.T. Lee, C.K. Ni, J. Chem. Phys. 123 (2005) 054309.
[26] G. Vall-llosera, M. Coreno, P. Erman, M.A. Huels, K. Jakubowska, A. Kivimaki, E. Rachlew, M. Stankiewicz, Int. J. Mass Spectrom. 275 (2008) 55–63.
[27] C.Q. Jiao, C.A. DeJoseph, R. Lee, A. Garscadden, Int. J. Mass Spectrom. 257 (2006) 34–40.
[28] B.E. Forch, S. Okajima, E.C. Lim, Chem. Phys. Lett. 108 (1984) 311–318.
[29] T. Beyer, D.F. Swinehar, Commun. ACM 16 (1973) 379.
[30] M.J. Frisch, G.W. Trucks, H.B. Schlegel, G.E. Scuseria, M.A. Robb, J.R. Cheeseman, J.J.A. Montgomery, T. Vreven, K.N. Kudin, J.C. Burant, J.M. Millam, S.S. Iyengar, J. Tomasi, V. Barone, B. Mennucci, M. Cossi, G. Scalmani, N. Rega, G.A. Petersson, H. Nakatsuji, M. Hada, M. Ehara, K. Toyota, R. Fukuda, J. Hasegawa, M. Ishida, T. Nakajima, Y. Honda, O. Kitao, H. Nakai, M. Klene, X. Li, J.E. Knox, H.P. Hratchian, J.B. Cross, C. Adamo, J. Jaramillo, R. Gomperts, R.E. Stratmann, O. Yazyev, A.J. Austin, R. Cammi, C. Pomelli, J.W. Ochterski, P.Y. Ayala, K. Morokuma, G.A. Voth, P. Salvador, J.J. Dannenberg, V.G. Zakrzewski, S. Dapprich, A.D. Daniels, M.C. Strain, O. Farkas, D.K. Malick, A.D. Rabuck, K. Raghavachari, J.B. Foresman, J.V. Ortiz, Q. Cui, A.G. Baboul, S. Clifford, J. Cioslowski, B.B. Stefanov, G. Liu, A. Liashenko, P. Piskorz, I. Komaromi, R.L. Martin, D.J. Fox, T. Keith, M.A. Al-Laham, C.Y. Peng, A. Nanayakkara, M. Challacombe, P.M.W. Gill, B. Johnson, W. Chen, M.W. Wong, C. Gonzalez, J.A. Pople, Gaussian 03, Gaussian, Inc., Pittsburgh, PA, 2003.
[31] K. Enomoto, J.A. LaVerne, S. Seki, S. Tagawa, J. Phys. Chem. A 110 (2006) 9874–9879.
[32] L. Poisson, K.D. Raffael, B. Soep, J.M. Mestdagh, G. Buntinx, J. Am. Chem. Soc. 128 (2006) 3169–3178.